Geochemical Perspectives Letters

A lunar hygrometer based on plagioclase-melt partitioning of water

Y.H. Lin, H. Hui, Y. Li, Y. Xu, W. van Westrenen

Supplementary Information

The Supplementary Information includes:

- 1. Experimental and Analytical Methods
- 2. Accuracy of Partition Coefficients
- 3. Oxygen Fugacity Calculations
- Tables S-1 and S-2
- Figures S-1 and S-2
- Supplementary Information References

1. Experimental and Analytical Methods

Starting Materials

The compositions of our starting materials and the experimental pressure-temperature conditions were based on an experimental study of LMO crystallisation, which has shown that plagioclase starts to crystallise after approximately 75% solidification of a bulk silicate Earth-like lunar magma ocean in water-bearing experiments (Lin *et al*., 2017a). The water-bearing bulk compositions that yielded plagioclase (steps LBS6H, LBS7H, and LBS8H from Lin *et al*. (2017a)) were chosen as starting compositions for our partitioning study. Starting materials were prepared by mixing appropriate amounts of high purity (99.5–99.99 %, Alfa Aesar) powdered (hydr)oxides (MgO, $Mg(OH)_2$, Fe_2O_3, Al_2O_3, $Al(OH)_3$, TiO_2, SiO_2) and $CaCO_3$ (99.95–100.05 %, Alfa Aesar). The oxides MgO, Al_2O_3, TiO_2 and SiO_2 were first fired overnight at 1000 °C and then stored at 110 °C until use. The other oxides, hydroxides and calcium carbonate were dried at 110 °C overnight prior to use. The nominally dry starting chemicals were mixed in ethanol using an agate mortar for 1 hour, and then the mixtures were dried in air and decarbonated in a Pt crucible in a box furnace by gradually raising the temperature from 650 to 1000 °C in approximately 7 hours. The Pt crucible had previously been iron-saturated to minimise iron loss. The mixtures were melted by heating to 1550 °C. The melts were kept at this high temperature for 20 minutes to promote homogeneity, and to reduce most of the iron in the starting material to Fe^{2+}. The melts were quenched to glass by immersing the bottom of the Pt crucible in water. The glass samples were subsequently crushed, dried, and ground in ethanol using an agate mortar for 1 hour and then kept at 110 °C until use. Water was added to nominally dry glass using $Mg(OH)_2$. The starting material compositions for water partitioning experiments, containing between 0.53 and 0.87 wt. % H_2O, are presented in Table S-1.

High-pressure Experiments

High-pressure, high-temperature partitioning experiments were performed in a piston cylinder press using a half-inch (12.7 mm) diameter talc-pyrex cell assembly (van Kan Parker *et al.*, 2011). For these experiments, a hand-machined graphite bucket with an inner diameter (ID) of 0.7 mm, outer diameter (OD) of ~1.7 mm, and a length of 3–4 mm, was filled with starting material, closed with a graphite lid and inserted in a gold-palladium ($Au_{80}Pd_{20}$) capsule, with an ID of 1.7 mm, OD of 2 mm, and a length of 5–7 mm. The bottom end of the $Au_{80}Pd_{20}$ capsule was triple crimped, flattened and welded shut. After the graphite capsule was inserted, the other end of the $Au_{80}Pd_{20}$ capsule was crimped and welded shut. The use of a graphite inner capsule ensures that the oxygen fugacities of these experiments are significantly lower than in previous studies focused on terrestrial conditions (Ulmer and Luth, 1991; see section 3 below). Temperatures were monitored using a W_5Re–$W_{26}Re$ (type C) thermocouple and Omega® CN76000 programmable controller. The sample center was located at the hotspot of the assembly, 2 mm away from the thermocouple tip end, so that the sample temperatures were within 10 °C of the thermocouple reading (Watson *et al.*, 2002). Experiments were pressurised cold and then heated to a superliquidus temperature of 1280 °C for 20 minutes. Subsequently, samples were cooled to the temperature of interest at a rate of 10 °C per hour while maintaining target pressure, and kept for 14–24 hours at target temperature. Target pressures were 0.3 or 0.4 GPa for all experiments conducted in this study, and final target temperatures ranged from 1160 to 1200 °C. At completion of each experiment, the sample assembly was quenched by cutting power to the heater and the temperature dropped below the glass transition temperature in <10 s.

Analytical Techniques and Procedures

Experimental run products were mounted in epoxy and polished into thick sections. The sections were carbon coated for back-scattered electron (BSE) imagery to assess texture and mineralogy and subsequent electron microprobe analysis (EMPA). The chemical compositions of the run product phases (minerals and quenched glasses) were determined using a JEOL JXA-8800M Electron Microprobe at Guangzhou Institute of Geochemistry, Chinese Academy of Sciences calibrated with primary standards of diopside (Ca, Si), fayalite (Fe), ilmenite (Ti), olivine (Mg) and orthoclase (Al). Analyses were carried out using an accelerating voltage of 15 kV and a beam current of 20 nA. Focused beams with 1 and 10 μm diameter were used for the mineral phases and quenched glasses, respectively. Peak count times were 20 seconds and background count times were 10 seconds. Compositions reported here are based on the average of 5–10 analyses. The modal abundances of all mineral and glass phases were determined using mass balance calculations, which agree well with the estimates derived from phase area percentages obtained using an EDAX-EDS system in imaging mode.

After EMPA analyses, carbon coatings were removed and experimental samples were doubly polished into sections with thicknesses ranging from 50 to 180 μm (measured with Mitutoyo thickness gauge) using abrasive paper and aluminum oxide powder. Subsequently, doubly-polished samples were successively cleaned using acetone, ethanol and deionised water in an ultrasonic cleaner, and then dried in air at room temperature. Finally, the dried sample sections were stored in a desiccator for 24 hours to eliminate potential water adsorbed on the surface of sample sections.

Water concentrations in minerals and coexisting glass in our samples were obtained at the State Key Laboratory for Mineral Deposits Research, Nanjing University, using a Continuμm microscope attached to a Nicolet IS50 Fourier transform infrared (FTIR) spectrometer. A liquid nitrogen cooled MCT/A detector and KBr beam splitter were used during FTIR analyses. The infrared light pathway was flushed with dried N_2 to minimise interference from atmospheric water vapor. Spectra (wavenumbers from 700 to 7000 cm^{-1}) with a resolution of 4 cm^{-1} were collected after 1024 scans for each FTIR analysis. Aperture sizes ranging from 50×50 μm to 15×15 μm were chosen on the basis of the dimensions of crystals and glass. Visible cracks were avoided to minimise possible contamination during FTIR measurements.

Water concentrations in analysed crystals and glass were calculated using the following equation according to the Beer-Lambert law:

$$c\ (\text{wt.}\%) = \frac{1.802 \cdot A_{\text{tot}}}{\rho \cdot t \cdot \varepsilon} \qquad \text{Eq. S-1}$$

where c is the water concentration of the mineral (wt. %), A_{tot} is the integral area under the absorption bands of interest on infrared spectra (cm^{-1}), ρ is the mineral density ($g \cdot cm^{-3}$), t is the sample thickness (cm), and ε is the integral molar absorption coefficient ($l \cdot mol^{-1} \cdot cm^{-2}$). Quantification of water concentrations in an anisotropic mineral normally requires analyses of oriented crystals using polarized light along the three principal optical directions. However, due to the difficulty of obtaining oriented plagioclase grains from the experimental charges, it was not possible to make measurements with a polarised infrared beam along the three principal axes of crystals. Therefore, the method using unpolarized infrared spectra of randomly oriented crystals (Kovács *et al.*, 2008; Sambridge *et al.*, 2008) was used to determine the water contents of our crystals. We have used the recently published water

absorption coefficient for Ca-rich plagioclase of 202600 ± 20260 l mol^{-1} cm^{-2} (Mosenfelder *et al.*, 2015) to convert infrared intensities to water contents in our anorthitic plagioclase crystals, and to enable comparison with previous work recalculated the previously published water concentrations of Ca-rich plagioclases from Hamada *et al.* (2013), in which an older estimate of the absorption coefficient of 107000 ± 5000 l mol^{-1} cm^{-2} (Johnson and Rossman, 2003) was used. A density of 2760 kg m^{-3} was used for plagioclase in Equation S-1.

To calculate water concentrations in silicate glass, the total absorbance A_{tot} is replaced by the peak height of the band at wavenumber ~3550 cm^{-1} on the unpolarised infrared spectra, and ρ is the density of basaltic glass (2819 kg·m^{-3} used in this study following Yamashita *et al.* (1997) and Hamada *et al.* (2013)). The molar absorption coefficient of 64 ± 1 l·mol^{-1}·cm^{-1} (Yamashita *et al.*, 1997) was used for basaltic glass.

2. Accuracy of Partition Coefficients

Plagioclase and glass compositions are very similar to those reported in Lin *et al.* (2017a) in terms of major and minor elements. In the absence of sodium and potassium, plagioclases are near-pure anorthite containing minor amounts of titanium, iron, and magnesium (Table S-2), and there is no obvious relationship between these elements and water content in our data. Glasses contain 45 ~ 49 wt. % SiO_2, typical for lunar magma ocean melts in equilibrium with plagioclase (Lin *et al.*, 2017a). Lengths and widths of the cross-sections of analysed plagioclase crystals range from 100 to 300 μm and from 50 to 150 μm, respectively (Fig. 1).

The plagioclase FTIR spectra in Fig. 2 are very similar to published spectra of natural plagioclase grains containing OH (Yang *et al.*, 2015; Liu *et al.*, 2018), in particular spectra of grains that were heated to high temperatures. The water absorption peaks in all glass samples are also centered at a wavenumber of ~3570 cm^{-1}. Furthermore, the H_2 bands, shown in the spectra of Yang *et al.* (2016), were not observed in our plagioclase spectra.

Because the water abundances in nominally anhydrous plagioclase are low, we performed multiple tests to confirm the absence of contamination of plagioclase analyses by silicate glass (that could be present as melt inclusions in grains or as melt pockets in micro-cracks underneath the surface of exposed plagioclase grains). The bands in Fig. 2 of the main manuscript are interpreted as absorption of structural O-H bond vibrations in plagioclase as opposed to vibrations in contaminant glass for two reasons. First, the OH absorbance measured at a single location in plagioclase grains changes systematically with the rotation of the infrared polariser relatively to the grain during FTIR measurements (Fig. S-1a,c,e). This is inconsistent with the sampling of amorphous glass contamination. In contrast, the OH absorbance in silicate glasses in our experiments remains constant with the rotation of the polariser (Fig. S-1b,d,f). This suggests that the broad band in plagioclase is not caused by contamination. Second, progressive thinning of the samples by repolishing, followed by re-analyses of the thinned samples, indicates that the OH absorbance in plagioclase and glass from our samples is always in linear proportion to sample thickness (Fig. S-2). This demonstrates that the plagioclase spectra are not affected by infrared absorption signals from heterogeneously distributed glass in the light path, nor can they represent combinations of spectra from multiple grains covering each other in the light path through the sample. The similarity between our spectra and previously published work (Johnson and Rossman, 2013; Yang *et al.*, 2015; Liu *et al.*, 2018), combined with the systematic variations in spectra taken at different polarisation angles and sample thicknesses, indicates that our plagioclase data are not affected by glass contamination.

In addition, the water partition coefficients reported by Caseres *et al*. (2017) of experiments at oxygen fugacities lower than those in most of our experiments ($D_{water}^{plag\text{-}melt}$ = 0.018–0.023 at the IW buffer) overlap with our results. The latter study used secondary ion mass spectrometry (SIMS), a time-resolved technique that excels at detecting inhomogeneities, to measure hydrogen abundances in plagioclase and melt. The excellent agreement between our results and these two literature studies lends further support to our conclusion that our plagioclase FTIR data do not suffer from contamination by glass.

3. Oxygen fugacity calculation

To calculate the oxygen fugacities in our experiments, based on our experimental assemblage with an outer-$Au_{80}Pd_{20}$ and inner graphite lining, we use Equation S-2a for the graphite–COH (C-COH) buffer (Ulmer and Luth, 1991) and Equation S-2b for the iron-wustite (IW) buffer (Frost, 1991) systems for iron metal bearing experiments:

$$\log fO_2 \text{ (C-COH buffer)} = (-22324 + 189 \cdot P - 1.41 \cdot P^2)/T + 4.62 \qquad \text{Eq. S-2a}$$

$$\log fO_2 \text{ (IW buffer)} = -27.489/T + 6.702 + 0.055 \cdot (1000 \cdot P - 1)/T \qquad \text{Eq. S-2b}$$

where T is the temperature (K), and P is the pressure (kbar). For the Hamada *et al*. (2013) and Caseres *et al.* (2017) experiments, the log(fO_2) was calculated using Frost (1991) for the NNO, FMQ, and IW systems. The calculated log(fO_2) values are shown in Table 1. Our experimental log(fO_2) values from eight samples at the C-COH buffer range from -10.0 to -10.4, which is ~2 log units above the IW buffer (Table 1), consistent with the absence of iron metal blebs in these experimental charges. The log(fO_2) of the single sample at the IW buffer is approximately -12.4 (Table 1), consistent with the presence of iron metal blebs in this experimental charge. The experiments for run products containing Fe-metal from Caseres *et al.* (2017) were performed at the IW buffer, at log(fO_2) = -12.3. The Hamada *et al.* (2013) experiments cover a range of log(fO_2) between -5.8 and -4.7. The fO_2 in our experiments is therefore ~6±2 log units lower than that in previous work focused on terrestrial compositions (Hamada *et al*., 2013), and overlaps with experimental data reported by Caseres *et al.* (2017) focusing on lunar crust formation.

Supplementary Tables

Table S-1 Nominal compositions of starting materials.

Experiment	SiO_2	TiO_2	Al_2O_3	FeO	MgO	CaO	Water (H_2O)	Total
Pl1_LBS6H	47.54	1.70	15.25	12.88	10.53	10.98	0.59	99.99
Pl2_LBS7H	47.96	1.88	15.68	12.52	9.53	11.19	0.66	100.01
Pl3_LBS8H_1	47.57	2.45	15.48	13.83	7.50	11.52	0.87	99.99
Pl4_LBS8H_2	47.57	2.45	15.48	13.83	7.50	11.52	0.87	99.99
Pl5_LBS8H_3	47.57	2.45	15.48	13.83	7.50	11.52	0.87	99.99
2018_Pl2_LBS8H	47.57	2.45	15.48	13.83	7.50	11.52	0.87	99.99
2018_Pl3_LBS7H	47.96	1.88	15.68	12.52	9.53	11.19	0.66	100.01
2018_Pl17_LBS8H	47.57	2.45	15.48	13.83	7.50	11.52	0.87	99.99
2018_Pl21_LBS5H	48.60	1.60	14.38	13.07	12.52	10.28	0.53	100.45

Compositions in wt. % oxides.

Table S-2 EMPA data of plagioclase and glass in experimental samples.

Experiment	Results								
	Phase	n	SiO_2	TiO_2	Al_2O_3	FeO	MgO	CaO	Total
Pl1_LBS6H	Plagioclase	7	45.59 (0.51)	0.15 (0.01)	33.31 (0.29)	1.23 (0.08)	0.89 (0.07)	18.73 (0.34)	99.9
	Glass	9	48.11 (0.82)	1.75 (0.04)	17.05 (0.19)	11.70 (0.39)	7.70 (0.16)	12.38 (0.17)	98.7
Pl2_LBS7H	Plagioclase	6	44.77 (0.44)	0.07 (0.01)	34.08 (0.32)	0.89 (0.07)	0.43 (0.03)	19.63 (0.37)	99.9
	Glass	10	47.35 (0.61)	1.82 (0.03)	17.54 (0.22)	11.96 (0.41)	7.48 (0.37)	13.24 (0.11)	99.4
Pl3_LBS8H_1	Plagioclase	5	46.07 (0.34)	0.08 (0.02)	33.38 (0.31)	0.81 (0.23)	0.46 (0.05)	19.04 (0.65)	99.8
	Glass	10	49.03 (0.75)	3.67 (0.05)	14.90 (0.17)	13.96 (0.35)	5.58 (0.18)	12.28 (0.31)	99.4
Pl4_LBS8H_2	Plagioclase	5	46.51 (0.49)	0.01 (0.01)	33.27 (0.65)	0.70 (0.16)	0.49 (0.06)	18.89 (0.44)	99.9
	Glass	10	49.45 (0.73)	3.19 (0.05)	15.23 (0.26)	13.49 (0.17)	5.52 (0.26)	12.40 (0.21)	99.3
Pl5_LBS8H_3	Plagioclase	8	46.11 (0.22)	0.03 (0.01)	33.46 (0.36)	0.66 (0.09)	0.41 (0.02)	18.89 (0.12)	99.6
	Glass	10	48.99 (0.46)	3.23 (0.04)	15.02 (0.13)	13.75 (0.48)	5.74 (0.33)	12.71 (0.22)	99.4

2018_Pl2_LBS8H	Plagioclase	5	45.96	0.01	33.91	0.58	0.59	18.86	99.9
			(0.33)	(0.01)	(0.35)	(0.06)	(0.03)	(0.32)	
	Glass	6	49.25	3.08	15.43	13.29	5.73	12.88	99.7
			(0.51)	(0.03)	(0.24)	(0.38)	(0.34)	(0.10)	
2018_Pl3_LBS7H	Plagioclase	6	44.79	0.11	34.42	0.73	0.55	19.40	100.0
			(0.38)	(0.02)	(0.41)	(0.21)	(0.05)	(0.35)	
	Glass	7	49.35	4.24	13.25	14.87	6.68	11.42	99.8
			(0.55)	(0.05)	(0.13)	(0.30)	(0.14)	(0.29)	
2018_Pl17_LBS8H	Plagioclase	7	45.89	0.02	33.81	0.56	0.48	18.79	99.6
			(0.42)	(0.01)	(0.26)	(0.07)	(0.02)	(0.19)	
	Glass	9	48.25	3.70	15.10	13.09	5.77	12.72	98.6
			(0.42)	(0.03)	(0.23)	(0.44)	(0.31)	(0.20)	
2018_Pl21_LBS5H	Plagioclase	7	45.90	0.08	33.39	0.89	0.70	18.97	99.9
			(0.59)	(0.01)	(0.55)	(0.17)	(0.06)	(0.42)	
	Glass	8	48.79	2.05	14.79	13.29	9.92	11.04	99.9
			(0.53)	(0.08)	(0.21)	(0.15)	(0.16)	(0.25)	

n, number of analyses; Compositions from EMPA in wt. % oxides with 1σ s.d. in parentheses.

Supplementary Figures

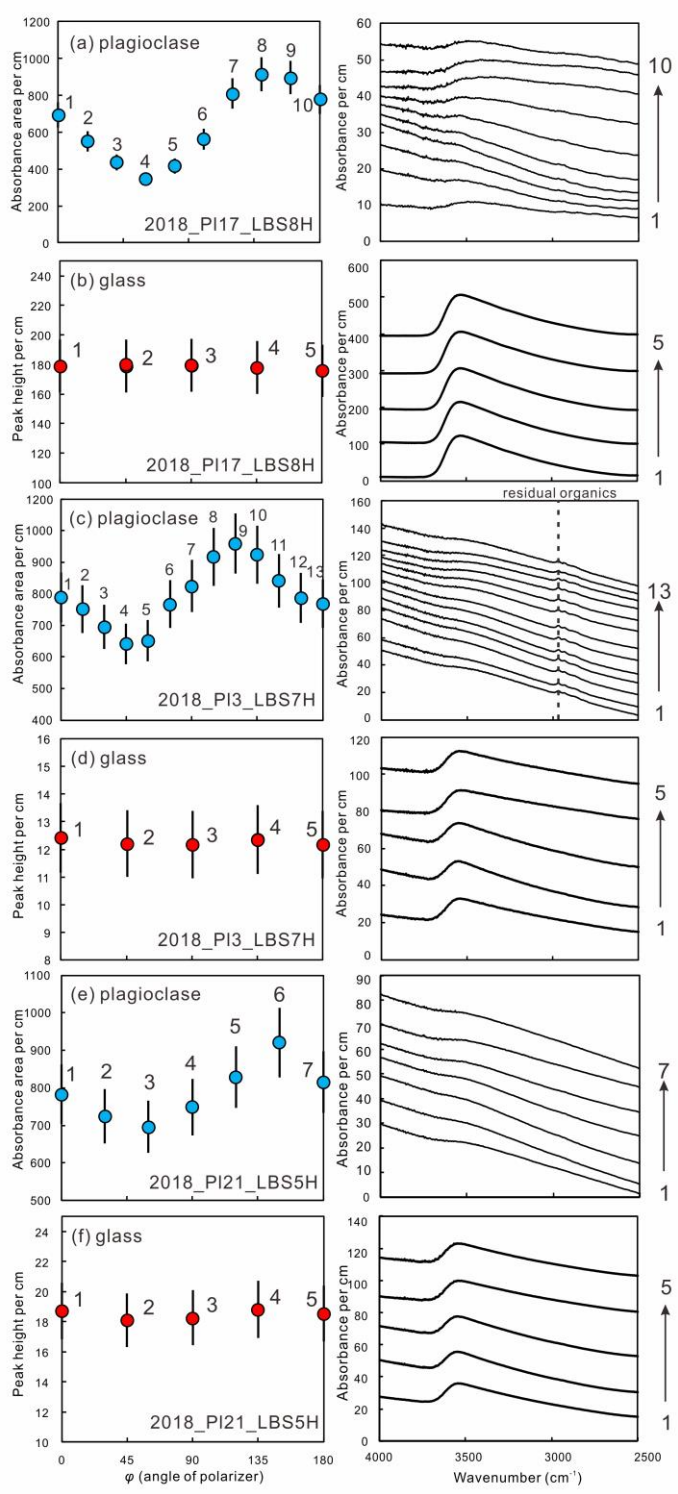

Figure S-1 Systematic variation in OH absorbance (area) of plagioclase **(a, c, e)** and constant OH absorbance (peak height) in glass **(b, d, f)** normalised to sample thickness of 1 cm with the angle of rotation of the infrared polariser, shown together with corresponding raw FTIR spectra**.** No grain was oriented relative to any major axis and the grain orientation was fixed during each series of measurements. FTIR measurements were conducted at a single location on each grain of plagioclase or glass by rotating the polariser relative to the grain orientation. Background measurements were taken in between each of the individual sample measurements. Filled circles show the absorbance calculated as the area beneath the O–H bands (~3600 to ~3000 cm^{-1}) for plagioclase and the absorbance expressed as the OH peak height for glass. Error bars represent ±10 % of the calculated absorbance. The narrow peaks (3000 to 2800 cm^{-1}) most probably come from residual organics on the grain surface during sample preparation.

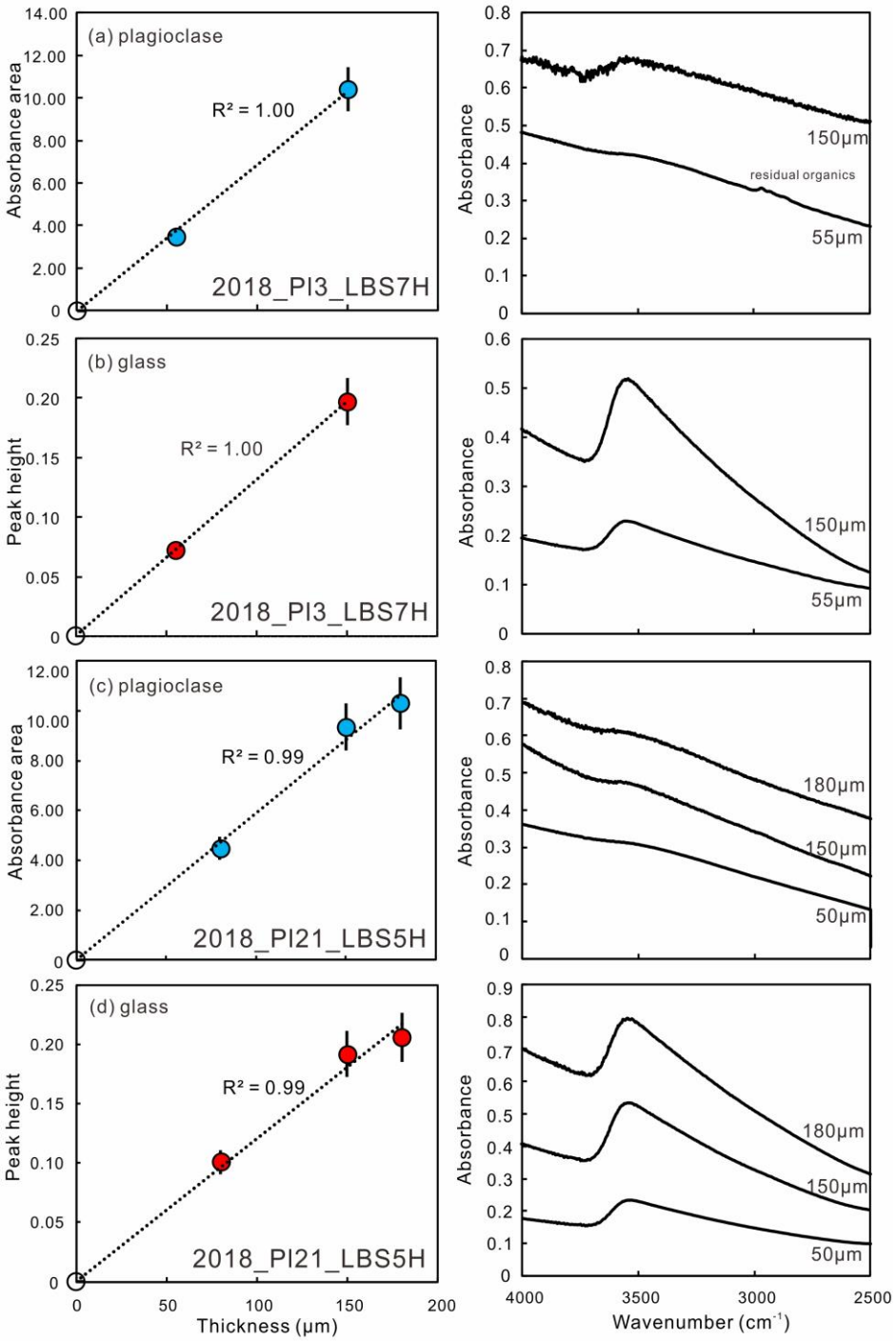

Figure S-2 Linear correlation between OH absorbance area in plagioclase **(a, c)** / peak height in glass **(b, d)** and grain thickness, with corresponding FTIR spectra**.** FTIR measurements were conducted at a single location on each grain / glass spot with the same orientation of the polarizer but different sample thickness. Error bars represent ±10 % of the absorbance.

Supplementary Information References

Caseres, J.R., Mosenfelder, J.L., Hirschmann, M.M. (2017) Partitioning of hydrogen and fluorine between feldspar and melt under the conditions of lunar crust formation. *Abstracts of the Lunar and Planetary Science Conference* 48, 2303.

Frost, B.R. (1991) Introduction to oxygen fugacity and its petrologic importance. *Reviews in Mineralogy and Geochemistry* 25, 1–9.

Hamada, M., Ushioda, M., Fujii, T., Takahashi, E. (2013) Hydrogen concentration in plagioclase as a hygrometer of arc basaltic melts: Approaches from melt inclusion analyses and hydrous melting experiments. *Earth and Planetary Science Letters* 365, 253–262.

Johnson, E.A., Rossman, G.R. (2013) The diffusion behavior of hydrogen in plagioclase feldspar at 800-1000°C: Implications for re-equilibration of OH in volcanic phenocrysts. *American Mineralogist* 98, 1779–1787.

Kovács, I., Hermann, J., O'Neill, H.S.C., Gerald, J.F., Sambridge, M., Horvath, G. (2008) Quantitative absorbance spectroscopy with unpolarized light: Part II. Experimental evaluation and development of a protocol for quantitative analysis of mineral IR spectra. *American Mineralogist* 93, 765–778.

Liu, W.D., Yang, Y., Zhu, K.Y., Xia, Q.K. (2018) Temperature dependences of hydrous species in feldspars. *Physics and Chemistry of Minerals* 45, 609–620.

Sambridge, M., Gerald, J.F., Kovács, I., O'Neill, H.S.C. (2008) Quantitative absorbance spectroscopy with unpolarized light: Part I. Physical and mathematical development. *American Mineralogist* 93, 751–764.

Ulmer, P., Luth, R.W. (1991) The graphite-COH fluid equilibrium in P, T, fO_2 space: An experimental determination to 30 kbar and 1600 °C. *Contributions to Mineralogy and Petrology* 106, 265–272.

Van Kan Parker, M., Mason, P.R.D., van Westrenen, W. (2011) Experimental study of trace element partitioning between lunar orthopyroxene and anhydrous silicate melt: Effects of lithium and iron. *Chemical Geology* 285, 1–14.

Watson, E.B., Wark, D.A., Price, J.D., van Orman, J. (2002) Mapping the thermal structure of solid-media pressure assemblies. *Contributions to Mineralogy and Petrology* 142, 640–652.

Yamashita, S., Kitamura, T., Kusakabe, M. (1997) Infrared spectroscopy of hydrous glasses of arc magma compositions. *Geochemical Journal* 31, 169–174.

Yang, X., Keppler, H., Li, Y. (2016) Molecular hydrogen in mantle minerals. *Geochemical Perspectives Letters* 2, 160–168.

Yang, Y., Xia, Q.K., Zhang, P.P. (2015) Evolutions of OH groups in diopside and feldspars with temperature. *European Journal of Mineralogy* 27, 185–192.